High-detection efficiency and low-timing jitter with amorphous superconducting nanowire single-photon detectors

Misael Caloz, Matthieu Perrenoud, Claire Autebert, Boris Korzh, Markus Weiss, Christian Schönenberger iD, Richard J. Warburton iD, Hugo Zbinden, and Félix Bussières

View Online   Export Citation   CrossMark

ARTICLES YOU MAY BE INTERESTED IN

Single-photon detectors combining high efficiency, high detection rates, and ultra-high timing resolution
APL Photonics **2**, 111301 (2017); https://doi.org/10.1063/1.5000001

Simple 2.5 GHz time-bin quantum key distribution
Applied Physics Letters **112**, 171108 (2018); https://doi.org/10.1063/1.5027030

Optically probing the detection mechanism in a molybdenum silicide superconducting nanowire single-photon detector
Applied Physics Letters **110**, 083106 (2017); https://doi.org/10.1063/1.4977034

High-detection efficiency and low-timing jitter with amorphous superconducting nanowire single-photon detectors

Misael Caloz,[1,a)] Matthieu Perrenoud,[1] Claire Autebert,[1] Boris Korzh,[1,b)] Markus Weiss,[2] Christian Schönenberger,[2] Richard J. Warburton,[2] Hugo Zbinden,[1] and Félix Bussières[1,3]

[1]*Group of Applied Physics, University of Geneva, CH-1211 Geneva, Switzerland*
[2]*Department of Physics, University of Basel, CH-4056 Basel, Switzerland*
[3]*ID Quantique SA, CH-1227 Carouge, Switzerland*

Recent progress in the development of superconducting nanowire single-photon detectors (SNSPDs) made of amorphous materials has delivered excellent performances and has had a great impact on a range of research fields. Despite showing the highest system detection efficiency (SDE) ever reported with SNSPDs, amorphous materials typically lead to lower critical currents, which have impacts on their jitter performance. Combining a very low jitter and a high SDE remains a challenge. Here, we report on highly efficient superconducting nanowire single-photon detectors based on amorphous MoSi, combining system jitters as low as 26 ps and a SDE of 80% at 1550 nm. We also report detailed observations on the jitter behaviour, which hints at intrinsic limitations and leads to practical implications for SNSPD performance. *Published by AIP Publishing.*
https://doi.org/10.1063/1.5010102

Since their first demonstration, superconducting nanowire single-photon detectors (SNSPDs) have emerged as a key technology for optical quantum information processing.[1,2] Their low dark count rate, fast response time, small jitter, and high efficiency favour their use in various demanding quantum optic applications such as quantum key distribution,[3] quantum networking,[4] device-independent quantum information processing,[5] deep-space optical communication,[6] and IR-imaging.[7,8] Notably, SNSPDs can be integrated in photonic circuits.[9,10]

One recent advance in the SNSPD field has been the introduction of amorphous superconductors such as tungsten silicide (WSi),[11] molybdenum silicide (MoSi),[12–14] and molybdenum germanium (MoGe).[15] SNSPDs based on these materials currently have the highest reported system detection efficiencies (SDEs) (93% for WSi[11]) and a high fabrication yield.[7]

The jitter of an SNSPD denotes the timing variation of the arrival time of the detection pulses. The jitter by itself is a crucial characteristic for time-resolved measurements such as light detection and ranging, high-speed quantum communication, and the lifetime measurement of single-photon sources. Typically, for a Gaussian distribution, the jitter is quantified using the full width at half maximum (FWHM) of the distribution. Despite showing the highest SDE ever reported with SNSPDs, amorphous materials operate at low bias currents and hence showed until now a time jitter rather high compared to what can be achieved with NbN[16–18] and NbTiN.[19] A wide range of values have been reported for different geometries and materials, typically from tens to hundreds of picoseconds. Some recently reported values range between ∼15 ps (NbN[16] and NbTiN[19]), ∼18 ps (NbN[17,18]), and 76 ps for the amorphous material (MoSi).[13]

In this work, we report on our results on the low timing jitter and high SDE of our MoSi SNSPDs. We measured the system jitters and SDE for several devices and obtained jitters (FWHM) as low as 26 ps and a saturated SDE of 80% or more at the telecom wavelength. We also report on detailed observations on the jitter behaviour, which hints at intrinsic limitations and leads to practical implications for SNSPD performance.

The SNSPDs are fabricated out of a 7 nm-thick film of amorphous $Mo_{0.8}Si_{0.2}$ deposited by co-sputtering with a DC and RF bias on the molybdenum and silicon targets, respectively. X-ray diffraction measurements have been performed, confirming the amorphous nature of MoSi. The fabrication is done in the following way: (i) a metallic mirror is evaporated on a thermally oxidised silicon wafer, (ii) a silicon dioxide (SiO_2) layer with a ∼λ/4 thickness is deposited by RF sputtering, and (iii) the MoSi film is deposited, capped with a 3 nm amorphous silicon (a-Si) layer, and covered by ∼50 nm of SiO_2. By choosing correctly the thickness of the two SiO_2 layers, constructive interference inside the structure maximises the absorption in the MoSi layer.[20] The film is patterned as a meandered wire covering a total surface area of 16×16 μm^2 by a combination of e-beam lithography and reactive ion etching. One wafer contains devices with different widths (100–180 nm) and fill factors (fraction of the active area). A self-aligning technique is used to ensure optimal coupling to the optical fibre.[21] The room temperature resistance of our devices is a few $M\Omega$, depending on the geometry of the nanowire and of the meander. The current density at I_{sat} is typically around 3 MA/cm^2 and is similar for all devices, more details can be found in the supplementary material.

The detectors are mounted in a sorption cryostat reaching 0.8 K. For measuring the jitter of the SNSPDs, a TCSPC module (Becker & Hickl, SPC-130) with a constant fraction discriminator (CFD) was set up, and a 6 ps (FWHM) pulse

---

width fibre laser (Nuphoton Technologies) at 1560 nm was used as the source, as shown in Fig. 1. The power of the source was attenuated to the single photon level by variable attenuators. The single-photon-response voltage pulse is amplified by a custom low-noise amplifier cooled to 40 K and by a secondary amplifier at room temperature. The cryogenic preamplifier is not necessary to operate the detectors, but it does provide a larger signal-to-noise ratio (SNR). The pulse polarity has no impact on the measured detector performances. For SNSPDs, the distribution of the intervals between the "Start" and the "Stop" signals typically shows a Gaussian profile, from which the system jitter can be extracted. The CFD of the TCSPC module ensures that the discrimination of the electrical pulse of the detector is done relative to its amplitude. For measuring the SDE, we used a continuous wave (CW) polarized laser at 1550 nm attenuated down to 10^5 photons/s by three variable attenuators in series and a calibrated power meter (see the supplementary material for more details). The input light polarization was set to optimize the number of counts of the SNSPDs. Figure 1 shows the schematic view for both jitter and SDE measurements. The measured jitter of the TCSPC module itself is 9 ps. We confirmed that our devices do not suffer from after pulsing by using a setup with a time to digital converter and a pulsed laser.

The SNSPD devices that we tested all have critical current above 30 μA, which results in detection pulses with large amplitudes. This greatly reduces the jitter component due to the noise, allowing us to reach very low jitters while keeping high efficiencies. We measured the system jitters and the SDE for tens of devices. At the operating temperature of 0.8 K and for 1550 nm, all tested devices exhibited a plateau region and very similar performances according to their designs, and all of them showed SDE >74% and system jitters <45 ps at the same time; selected devices for this paper are shown in Table I. In particular, we obtained a device combining a system jitter as low as 26 ps (FWHM) for a SDE of 80.1% ± 0.9% as shown in Fig. 2 and another one combining a SDE of 85.8% ± 0.9% and a system jitter of 44 ps. The DCR of ≤ 1000 cps, mainly due to the black body radiation, can be significantly reduced by installing fibre based filters. The uncertainty on the efficiency measurement has been estimated by an error propagation calculation, and details on the computation are explained in the supplementary material.

The measured system timing jitter j_{sys} can be decomposed into three main parts: (i) a noise component coming from the

TABLE I. List of selected devices with their characteristics.

Detector	Width (nm)	Fill factor	SDE (%)	Jitter (ps)
#1	150	0.7	85.8	44.2
#2	150	0.7	82.3	35.4
#3	160	0.6	80.2	32.7
#4	150	0.6	76.5	30.1
#5	160	0.5	80.1	26.1
#6	150	0.5	74.6	28.6

electronic readout noise, (ii) a setup component from the laser pulse width and TCSPC module, and (iii) a component which is intrinsic to the detection process (hotspot dynamic and geometric effect[8]). Improving the detector pulse amplitude has significantly decreased the noise-induced jitter component, allowing us to observe intrinsic jitter behaviour which was not accessible until now with amorphous materials. While the two first components are well-known contributions, it remains unclear how the intrinsic jitter contributes to j_{sys}.[17,22] The spread of the reported system jitter values in the literature makes it difficult to determine the origin of the intrinsic jitter of a device quantitatively, and the mechanism of this intrinsic jitter is still not completely understood.[17,22–24] By analysing the bias current dependence of the system jitter for several devices, we can extract the contribution of the intrinsic jitter and reveal its behaviour as the detector efficiency reaches saturation. Assuming that the noise (j_{noise}), intrinsic (j_{int}), and setup (j_{setup}) contributions to the system jitter are independent,[17,22] we can write the system jitter as

$$j_{sys} = \sqrt{j_{noise}^2 + j_{setup}^2 + j_{int}^2}, \qquad (1)$$

where the intrinsic jitter itself is a combination of the jitter coming from the hotspot dynamics and the geometric effects, $j_{int} = \sqrt{j_{hotspot}^2 + j_{geometric}^2}$. Here, $j_{hotspot}$ and $j_{geometric}$ cannot be estimated independently. Nevertheless, the intrinsic jitter j_{int} can be estimated if the other contributions are known: j_{setup} is given by the laser specification sheets and by the TCSPC module measurement, while the noise-induced jitter (j_{noise}) was estimated from

$$j_{noise} = 2\sqrt{2\ln(2)}\frac{\sigma_{RMS}}{SR}, \qquad (2)$$

where σ_{RMS} is the RMS value of the electronic noise and SR is the slew rate of the electrical pulse coming from a
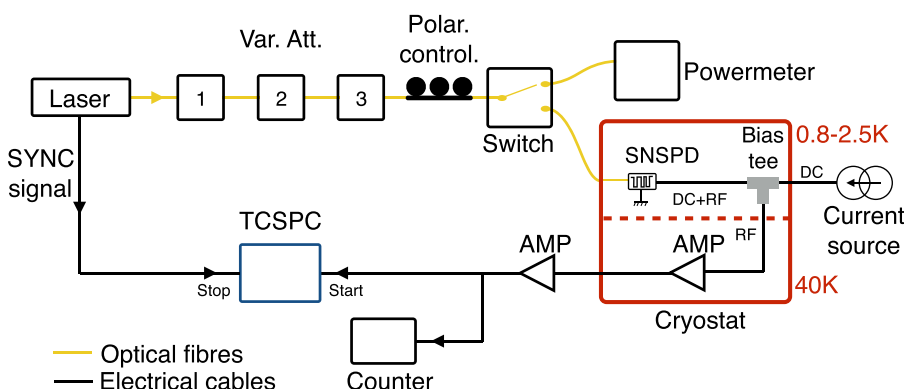

FIG. 1. Schematic view of the setup for measuring both the system jitter and the efficiency of the SNSPDs. For the jitter and SDE measurement, the counter and TCSPC modules were not used, respectively.
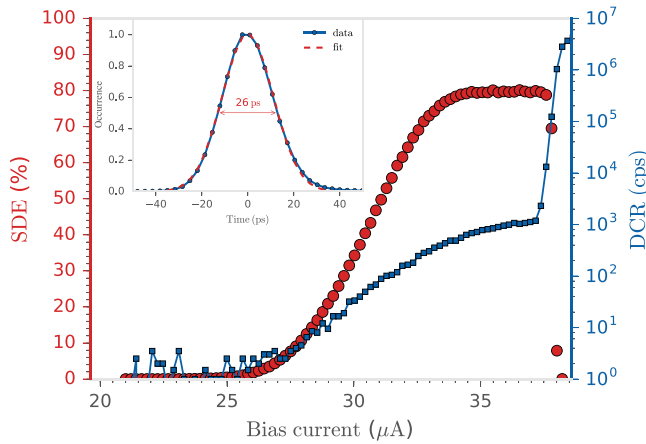
FIG. 2. System detection efficiency (red circles) and the dark count rate (blue squares) as a function of the bias current for device #5, at 1550 nm and 0.8 K. Error bars are too small to be seen. Inset: System jitter for the same device at $I_b = 37$ μA, the blue and red lines indicate the data and the Gaussian fit, respectively. The system jitter measured is 26 ps (FWHM) and is indicated by the double arrow.

detection event in the SNSPD, both measured on an oscilloscope having a 6 GHz bandwidth, and more details can be found in the supplementary material.

Figure 3 shows the evolution of the system jitter as a function of the bias current for different devices listed in Table I. In order to compare them, the bias current is normalized to the saturation current (I_{sat}), which we defined as the bias current at which the SDE reaches 90% of its maximum value at the plateau. The jitter values for devices #1 and #2 are higher than for the other ones. These devices have a higher fill-factor and are also longer. Their larger jitter could possibly be attributed to a larger geometric effect although this cannot be confirmed from these measurements alone. We plotted the different system jitter components using Eqs. (1) and (2) for device #4 in Fig. 4.

For high bias currents, the noise-induced jitter becomes very small, and an improvement in the amplification chain could possibly reduce it even more,[18,22] which could potentially lead to system jitters below 20 ps. We note that the
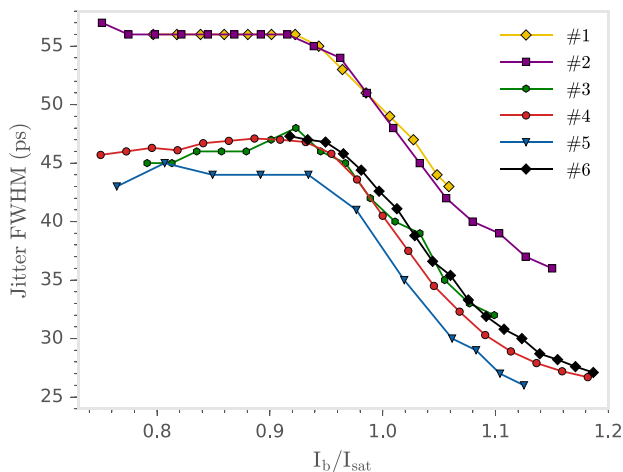

FIG. 3. Jitter (FWHM) as a function of I_b normalized to the saturation current (I_{sat}) for different devices shown in Table I. Here, I_{sat} is defined as the bias current at which the SDE reaches 90% of its maximum. Error bars are too small to be seen.
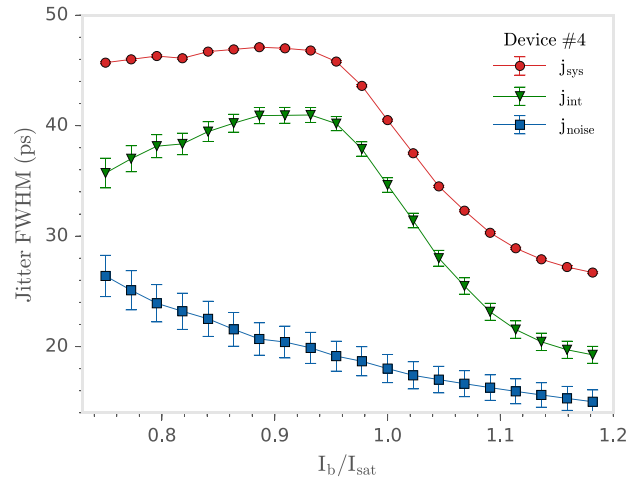

FIG. 4. Different jitter components (FWHM) as a function of I_b normalized to the saturation current (I_{sat}) for device #4 with their error bars. The coloured lines represent the different jitter components in the following way; red: measured system jitter, blue: estimated noise-induced jitter using Eq. (2), and green: computed intrinsic jitter using Eq. (1).

intrinsic jitter j_{int} strongly depends on the applied bias current. From Figs. 3 and 4, for all devices (with different widths, lengths, and fill factors), the following points can be highlighted: (i) j_{sys} is a constant for low bias currents, (ii) j_{sys} exhibits the same inflexion point close to $\sim 0.92 \, I_{sat}$, (iii) by increasing the bias current above the inflexion point, the system and intrinsic jitters decrease significantly, and (iv) the jitter flattens close to $\sim 1.2 \, I_{sat}$ and could potentially reach an optimal value. These observations are relevant for studying the detection mechanism in SNSPDs,[25] but this analysis is beyond the scope of this study and is left for future work. Points (iii) and (iv) have implications for SNSPD performances, namely, that operation well into the plateau ($I_b > I_{sat}$) is necessary to reach an optimal jitter value.

Interestingly, the jitter histogram of all tested devices is asymmetric and non-Gaussian in the vicinity of I_{sat}. Figure 5 shows such a distribution measured at $I_b = I_{sat}$. The asymmetry consists of a long exponentially decaying tail after the maxima of the histogram. This is the "transition" region between the "probabilistic" regime, where the absorption of a photon leads to a resistive region with a small probability, and the "deterministic" regime (the plateau), where photon absorption leads to a resistive region with almost certainty. The asymmetry however mostly disappears outside of the transition region, where it tends to be much more Gaussian. The same observations have recently been reported and discussed in a theoretical framework to understand better the detection mechanism in SNSPDs.[25] The first inset of Fig. 5 shows the system jitter at 20 dB $j_{sys}(-20 \text{ dB})$ below the maxima of the histogram. To highlight the non-Gaussian behaviour, the residues between $j_{sys}(-20 \text{ dB})$ and the Gaussian distribution are shown on the second inset. Given that the setup (j_{setup}) and noise (j_{noise}) jitter distributions are Gaussian, this evolution of the asymmetry can only be explained by an intrinsic contribution. From an application point of view, it is clear here too that the optimal SNSPD operation [$j_{sys}(\text{FWHM})$ and $j_{sys}(-20 \text{ dB})$] is reached when the bias current is greater than $\sim 1.1 \, I_{sat}$. This means again that a detector with a very large deterministic region will
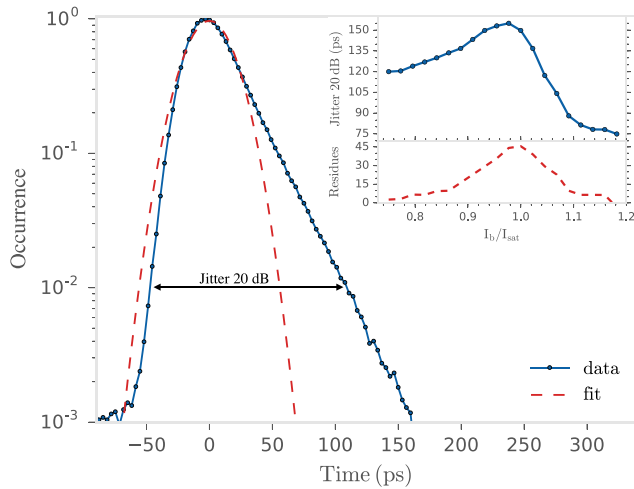
FIG. 5. System jitter distribution on a logarithmic scale at a bias current equal to I_{sat}. The blue and red lines represent the data and the Gaussian fit, respectively. The double arrow indicates where the system jitter at –20 dB $j_{sys}(-20\,\text{dB})$ is extracted. Inset: $j_{sys}(-20\,\text{dB})$ and its residues from what is expected with a Gaussian distribution [residues = $j_{sys}(-20\,\text{dB}) - j_{gauss}(-20\,\text{dB})$]. Error bars are too small to be seen.

show intrinsically better performances in terms of both $j_{sys}(-20\,\text{dB})$ and $j_{sys}(\text{FWHM})$. This point is particularly relevant for applications where a low $j_{sys}(-20\,\text{dB})$ is mandatory,[26] such as quantum key distribution and time-resolved measurements, where the visibility of a Bell state measurement on photonic qubits created at random times will be directly affected by the ability of the detectors to resolve the arrival time of the photons.[4]

In conclusion, we reported on highly efficient superconducting nanowire single-photon detectors based on amorphous MoSi operating at 0.8 K combining a system jitter as low as 26 ps and a SDE greater than 80% at 1550 nm at the same time. We achieved high bias currents, and we showed that the timing jitter is limited by noise and by an intrinsic component. The observations of its behaviour indicate that the system jitter might reach an optimal value for a high bias current value, hinting at an intrinsic limit. A non-Gaussian tail increasing the system jitter at –20 dB has also been observed and quantified, having direct implications for applications such as quantum key distribution where low jitters are crucial. Our results, and in particular the fact that we can study the jitter behaviour well into the plateau, could lead to insights into the study of the detection mechanism in SNSPDs.[25,27] In this work, we could not isolate the contribution of the geometric jitter from the one due to hotspot dynamics. This could be attempted by using either a double-ended readout amplifier[22] or detectors made of a very short wire. Such studies are left for future work.

See supplementary material for details of the SDE uncertainty computation, the noise and setup jitter decomposition, and the superconducting MoSi film properties.

[1]G. N. Gol'tsman, O. Okunev, G. Chulkova, A. Lipatov, A. Semenov, K. Smirnov, B. Voronov, A. Dzardanov, C. Williams, and R. Sobolewski, Appl. Phys. Lett. **79**, 705 (2001).
[2]R. H. Hadfield, Nat. Photonics **3**, 696 (2009).
[3]H. Takesue, S. W. Nam, Q. Zhang, R. H. Hadfield, T. Honjo, K. Tamaki, and Y. Yamamoto, Nat. Photonics **1**, 343 (2007).
[4]F. Bussières, C. Clausen, A. Tiranov, B. Korzh, V. B. S. W. Nam, F. Marsili, A. Ferrier, P. Goldner, H. Herrmann, C. Silberhorn, W. Sohler, M. Afzelius, and N. Gisin, Nat. Photonics **8**, 775 (2014).
[5]L. K. Shalm, E. Meyer-Scott, B. G. Christensen, P. Bierhorst, M. A. Wayne, M. J. Stevens, T. Gerrits, S. Glancy, D. R. Hamel, M. S. Allman, K. J. Coakley, S. D. Dyer, C. Hodge, A. E. Lita, V. B. Verma, C. Lambrocco, E. Tortorici, A. L. Migdall, Y. Zhang, D. R. Kumor, W. H. Farr, F. Marsili, M. D. Shaw, J. A. Stern, C. Abellán, W. Amaya, V. Pruneri, T. Jennewein, M. W. Mitchell, P. G. Kwiat, J. C. Bienfang, R. P. Mirin, E. Knill, and S. W. Nam, Phys. Rev. Lett. **115**, 250402 (2015).
[6]M. Shaw, K. Birnbaum, M. Cheng, M. Srinivasan, K. Quirk, J. Kovalik, A. Biswas, A. D. Beyer, F. Marsili, V. Verma, R. P. Mirin, S. W. Nam, J. A. Stern, and W. H. Farr, in *CLEO: 2014* (Optical Society of America, 2014), p. SM4J.2.
[7]M. S. Allman, V. B. Verma, M. Stevens, T. Gerrits, R. D. Horansky, A. E. Lita, F. Marsili, A. Beyer, M. D. Shaw, D. Kumor, R. Mirin, and S. W. Nam, Appl. Phys. Lett. **106**, 192601 (2015).
[8]Q.-Y. Zhao, D. Zhu, N. Calandri, A. E. Dane, A. N. McCaughan, F. Bellei, H.-Z. Wang, D. F. Santavicca, and K. K. Berggren, Nat. Photonics **11**, 247 (2017).
[9]J. P. Sprengers, A. Gaggero, D. Sahin, S. Jahanmirinejad, G. Frucci, F. Mattioli, R. Leoni, J. Beetz, M. Lermer, M. Kamp, S. Höfling, R. Sanjines, and A. Fiore, Appl. Phys. Lett. **99**, 181110 (2011).
[10]P. Rath, O. Kahl, S. Ferrari, F. Sproll, G. Lewes-Malandrakis, D. Brink, K. Ilin, M. Siegel, C. Nebel, and W. Pernice, Light: Sci. Appl. **4**, e338 (2015).
[11]F. Marsili, V. B. Verma, J. A. Stern, S. Harrington, A. E. Lita, T. Gerrits, I. Vayshenker, B. Baek, M. D. Shaw, R. P. Mirin, and S. W. Nam, Nat. Photonics **7**, 210 (2013).
[12]Y. P. Korneeva, M. Y. Mikhailov, Y. P. Pershin, N. N. Manova, A. V. Divochiy, Y. B. Vakhtomin, A. A. Korneev, K. V. Smirnov, A. G. Sivakov, A. Y. Devizenko, and G. N. Goltsman, Supercond. Sci. Technol. **27**, 095012 (2014).
[13]V. B. Verma, B. Korzh, F. Bussières, R. D. Horansky, S. D. Dyer, A. E. Lita, I. Vayshenker, F. Marsili, M. D. Shaw, H. Zbinden, R. P. Mirin, and S. W. Nam, Opt. Express **23**, 33792 (2015).
[14]M. Caloz, B. Korzh, N. Timoney, M. Weiss, S. Gariglio, R. J. Warburton, C. Schönenberger, J. Renema, H. Zbinden, and F. Bussières, Appl. Phys. Lett. **110**, 083106 (2017).
[15]V. B. Verma, A. E. Lita, M. R. Vissers, F. Marsili, D. P. Pappas, R. P. Mirin, and S. W. Nam, Appl. Phys. Lett. **105**, 022602 (2014).
[16]J. Wu, L. You, S. Chen, H. Li, Y. He, C. Lv, Z. Wang, and X. Xie, Appl. Opt. **56**, 2195 (2017).
[17]L. You, X. Yang, Y. He, W. Zhang, D. Liu, W. Zhang, L. Zhang, L. Zhang, X. Liu, S. Chen, Z. Wang, and X. Xie, AIP Adv. **3**, 072135 (2013).
[18]V. Shcheslavskiy, P. Morozov, A. Divochiy, Y. Vakhtomin, K. Smirnov, and W. Becker, Rev. Sci. Instrum. **87**, 053117 (2016).
[19]I. E. Zadeh, J. W. Los, R. B. Gourgues, V. Steinmetz, G. Bulgarini, S. M. Dobrovolskiy, V. Zwiller, and S. N. Dorenbos, APL Photonics **2**, 111301 (2017).
[20]V. Anant, A. J. Kerman, E. A. Dauler, J. K. W. Yang, K. M. Rosfjord, and K. K. Berggren, Opt. Express **16**, 10750 (2008).
[21]A. J. Miller, A. E. Lita, B. Calkins, I. Vayshenker, S. M. Gruber, and S. W. Nam, Opt. Express **19**, 9102 (2011).
[22]N. Calandri, Q.-Y. Zhao, D. Zhu, A. Dane, and K. K. Berggren, Appl. Phys. Lett. **109**, 152601 (2016).
[23]Q. Zhao, L. Zhang, T. Jia, L. Kang, W. Xu, J. Chen, and P. Wu, Appl. Phys. B **104**, 673 (2011).
[24]J. A. O'Connor, M. G. Tanner, C. M. Natarajan, G. S. Buller, R. J. Warburton, S. Miki, Z. Wang, S. W. Nam, and R. H. Hadfield, Appl. Phys. Lett. **98**, 201116 (2011).
[25]M. Sidorova, A. Semenov, H.-W. Hubers, I. Charaev, A. Kuzmin, S. Doerner, and M. Siegel, Phys. Rev. B **96**, 184504 (2017).
[26]E. Amri, G. Boso, B. Korzh, and H. Zbinden, Opt. Lett. **41**, 5728 (2016).
[27]A. Engel, J. Renema, K. Il'in, and A. Semenov, Supercond. Sci. Technol. **28**, 114003 (2015).